Flight Testing GBAS for UAV Operations

Michael Felux, Sophie Jochems, Philipp Schnüriger, Valentin Fischer, Patrick Steiner (Zurich University of Applied Sciences, Center for Aviation), Michael Jäger, Luciano Sarperi (Zurich University of Applied Sciences, Institute of Signal Processing and Wireless Communications)
Natali Cacciopoli (Eurocontrol)

Abstract
In this study the concept of using GBAS corrections and integrity parameters for UAV operations is explored. The GBAS messages are received and decoded at the airport to overcome the issue of VDB coverage for alternative applications that do not have line-of-sight to the GBAS. A flight test at a distance of about 15 km from an operational GBAS ground station was conducted using a quad-rotor UAV as test vehicle. The recorded GBAS messages and recorded pseudoranges and carrier phases were subsequently used to evaluate the performance that can be obtained. One main issue that was identified is the number of satellites lost when maneuvering the drone. Loss of tracking requires a re-initialization of the smoothing filter and thus entails a wait time before a satellite can be used for positioning again. The GBAS corrections are generated based on 100 s smoothing, requiring a user to use the same smoothing time constant do avoid potential differential error buildups due to different filters. Hence, the time until a satellite can be used again after reacquisition may be substantial. When losing several satellites simultaneously or shortly after another this decreases the number of available satellites significantly and negatively impacts accuracy and protection level performance of this proposed mode of operation. The paper also studies the multipath effect at different altitudes and for different smoothing time constants compared to the standardized error models that were defined for large transport aircraft. When using 100 s smoothing the results indicate that the models are suitable also for the use case of UAV operations.

1. INTRODUCTION

The Ground Based Augmentation System (GBAS) is a precision approach and landing system which provides corrections for GPS navigation signals to airborne users. Together with those corrections, it provides integrity parameters allowing users to bound their residual position errors after applying the corrections to the pseudorange measurements of the airborne user equipment. Finally, the station also provides reference coordinates defining the reference approach trajectory guiding aircraft horizontally and vertically towards the runway. All data are broadcast from the ground station via a VHF data broadcast (VDB) in a standardized format specified in DO-246E (RTCA, 2017a). The broadcast is freely accessible and can therefore be received and decoded by virtually everyone. A GBAS ground station is located within the security perimeter of an airport, uses high-quality antenna and receiver equipment that allows keeping errors introduced by the ground facility itself to a minimum. Furthermore, it provides guaranteed levels of performance according to specification and continuously self-monitors the integrity of the information provided (RTCA, 2017b).

This augmentation system, by design only serves a very specific purpose: in civil aviation, aircraft equipped with the appropriate avionics can use the provided information to correct GPS signals, ensure that all integrity requirements are met, and use the information regarding the approach geometry in the GBAS message to fly precision approaches. However, GBAS to date is not very widely used because i) not many airports are equipped with a GBAS ground station and ii) depending on the airport, not much of the fleet operating in and out is equipped with the GBAS landing system (GLS). The reason for this is a classic chicken/egg problem: On the one hand, the Air Navigation Service Provider (ANSP), or in some cases also the airport operator, is responsible for the installation, operation and maintenance of a GBAS ground station. As this is rather expensive, not many ANSPs and/or airports are willing to install such a ground station without a solid business case. As often only a small percentage of aircraft operating at a particular airport are equipped to fly a GLS approach, it is currently still very difficult to generate operational benefits from a GBAS. On the other hand, there are the aircraft operators. For them, it is also financially not very rewarding to equip their aircraft with the required receiver as there may be only a few destinations within their network where flying a GLS approach is possible and might bring operational benefits eventually.

In previous work Pullen et al. (2013a, 2013b) already explored the possibilities of using GBAS-like Local Area Differential GNSS (LADGNSS), that is similar in nature to GBAS but removes some expensive hardware making it more suitable to support UAV

operations while still providing high levels of integrity. As identified in this work and followed up upon by Kim et al. (2015), airborne multipath errors play a critical role for integrity. But it was shown in flight trials with UAVs that the residual airborne multipath errors are well bounded by the error models developed for large transport aircraft (Murphy et al., 2005; Circiu et al., 2020). In our previous work, Jochems et al. (2022) analyzed the performance of the envisioned Differentially Corrected Positioning Service (DCPS) for GBAS, a service type that enables other use-cases than precision approach guidance of large aircraft but relying on an actual GBAS. For that purpose, GBAS messages transmitted by the operational ground station at Zurich airport (ZRH) were received and decoded. The theoretical protection levels at different distances from the ground station for the GBAS DCPS were then calculated and compared to the SBAS protection levels. The results have shown that the use of GBAS could provide operational benefits when staying within a radius of around 57 km from the airport. At distances more than 57 km away from the airport, the GBAS protection levels become larger than the SBAS protection levels due to ionospheric and ephemeris error decorrelation and therefore no longer provide any advantage over the use of SBAS.

In this paper we continue our previous work and focus on the use of GBAS corrections in the emerging field of UAV navigation at distances below 50 km from the ground station. One main challenge when intending to use the broadcast corrections is the limited possibility to receive the VHF-based transmission at the low flight altitudes typical for this kind of operations. The concept explored in this work is therefore the reception and decoding of the GBAS messages at a location close to the airport and the application of the corrections and use of the integrity parameters for correcting and bounding the positioning errors at the UAV. We evaluate the performance of the proposed navigation method and discuss operational aspects of GNSS navigation for UAV operations.

2. METHODS

To evaluate performance under realistic conditions we conducted a flight test using a UAV and the recorded corrections and integrity parameters from operational GBAS at Zurich airport for subsequent postprocessing. This section describes the measurement setup and the performance metrics used for the evaluations.

2.1 DATA COLLECTION

For obtaining the GBAS corrections, a software-defined radio receiver was set up near the airport of Zurich with its operational GBAS Approach Service Type (GAST) C GBAS station. The selected location was within line-of-sight to the VDB transmit antenna and thus good signal reception was ensured (see left part of Figure 1). The GBAS in Zurich was in regular operation at the time of recording, provided corrections and integrity parameters for the approach service and is supporting CAT-I operations (i.e. operations down to 200 ft above ground) to Runway 14, the main landing runway. While a fully operational concept would require near real-time decoding and forwarding of the GBAS data via the cell phone network, for this initial study we recorded the GBAS data for later postprocessing together with the GNSS data from the UAV.

Figure 1 *Left: GBAS VDB message recording at Zurich Airport, GBAS transmit antenna location is marked with red cross; Right: DJI Matrice used for flight test in Winterthur. Red arrow shows GNSS antenna position and GNSS receiver mount.*

The UAV used in this test was a DJI Matrice (see right part of Figure 1). It was flown at a glider airfield in Winterthur, approximately 15 km away from Zurich airport. Onto the drone we mounted a Septentrio Development Kit receiver with a GNSS antenna on a 3D-printed case attached rigidly to the airframe. The receiver was recording GPS and Galileo pseudorange and carrier phase information on L1/E1 and L5/E5a, as well as SBAS information. As GBAS and SBAS are both only providing corrections and integrity parameters for the L1 signal of GPS, only this information was used for the performance evaluations in this study. Dual frequency measurements were used to remove the ionospheric divergence in the multipath estimation process (see section 2.3). The flight test contained periods of static hovering at altitudes of 2 m and 5 m above ground to collect GNSS data in a stationary scenario but at different altitudes for an initial assessment of the potential impact of ground reflection multipath at different heights above ground. Due to limited battery power the hovering periods lasted for around 10 minutes per altitude. Next, the UAV was flown in a more dynamic way in a rectangular shape. The purpose of this test was to investigate the effects of frequent changes in the attitude of the drone. At each corner we were hovering for about 3 minutes to give the receiver time to reacquire potentially lost satellites.

2.2 NUMBER OF USABLE SATELLITES

A property that is substantially different when flying UAVs compared to large fixed-wing aircraft, is the much higher dynamic and the significantly larger attitude angles that drones experience in flight. Thus, also the GNSS antenna (if attached rigidly to the airframe) is tilted and may lose track of satellites that fall below the antenna horizon when maneuvering. A loss of track of certain satellites typically requires the smoothing filter to be re-initialized. Depending on the filter implementation and the associated bounding methods, it may take up to 3.6 times the smoothing filter time constant until the re-acquired satellite is re-incorporated into the position solution. Hence, the number of usable satellites in the position solution may be significantly lower than the number of visible satellites and thus lead to poorer geometries and larger protection levels. Since the filter convergence time depends on the smoothing time constant, the potential impact of reduced smoothing times for faster re-incorporation of satellites into the position solution is investigated.

2.3 AIRBORNE MULTIPATH ASSESSMENT

One important input for the integrity assessment and the protection level calculation (see section 2.4) is the expected airborne multipath. For classical GBAS operations it is modeled by an exponential function that is dependent on satellite elevation, correlator spacing and bandwidth of the receiver and the smoothing time constant as was shown by Circiu et al., (2020). However, this model is based only on airborne measurements from large transport aircraft. As the multipath environment for UAVs may differ due to lower flying altitudes with the potential for ground reflections and significantly different reflection characteristics of the airframe, we collected airborne data while the UAV was hovering stationary at two different heights. While the amount of data collected in samples of just 10 minutes is certainly not enough to develop reliable models, the purpose within this study was to compare the measurements obtained to the standardized airborne multipath models and determine if the order of magnitude of the airborne multipath on UAVs is similar. For assessing the multipath, first two Hatch smoothing filters with smoothing time constants of 100 s and 10 s were applied to the pseudorange measurements on the L1 frequency (Hatch, 1983). Second, the code-minus-carrier (CMC) method with removal of the ionospheric divergence was performed. The data obtained was then levelled to zero mean and an elevation mask of 5 ° was applied to the data. The process is described in much greater detail e.g. in Circiu et al. (2020) and can be formulated as

$$MP_{L1} = \rho_{L1} - \phi_{L1} - 2\frac{f_{l5}^2}{f_{L1}^2 - f_{L5}^2}(\phi_{L1} - \phi_{L5}) \tag{1}$$

where ρ is the code measurement, ϕ are the carrier phase measurements, f the center frequencies of the navigation signals and the subscripts indicating the respective frequency band of the measurements. The evaluations were done separately for the data collected at 2 m and 5 m above ground. In order to compare the results for the two heights and two different smoothing time constants, i) the standard deviation of the multipath estimates per satellite as a function of its average elevation over the measurement period was calculated and ii) σ_{air} from the standardized airborne multipath model (RTCA, 2017b) was compared against the CMC data.

2.4 GBAS AND SBAS PERFORMANCE EVALUATION

Finally, the observed airborne navigation performance of the GBAS and SBAS corrected positioning solutions are compared in terms of accuracy, using a post-processed reference trajectory. This reference was calculated as a differential carrier phase solution relative to a fixed installation on the rooftop of the university building located at a distance of about 4 km from the test area. The GBAS and SBAS position solutions are computed using Eurocontrol's PEGASUS software, a toolset allowing the calculation of a variety of different GNSS-based navigation solutions compliant with the applicable aviation standards. Along with the position

solutions, PEGASUS also outputs the respective protection levels. The protection levels for SBAS according to the Minimum Operational Performance Standards (MOPS) DO-229F (RTCA, 2020) were used in this study. The horizontal protection levels for the GBAS positioning service ($HPL_{GBAS,pos}$) were calculated based on the DO-253D (RTCA, 2017b) and using the information from PEGASUS which satellites were used and the transmitted integrity parameters from the GBAS message as the maximum of the nominal protection level (HPL_{H0}), the faulted protection level (HPL_{H1}) and the horizontal ephemeris error protection bound (HEB)

$$HPL_{GBAS,pos} = \max\left(HPL_{H0}, HPL_{H1}, HEB\right) \tag{2}$$

with

$$HPL_{H0} = K_{ffmd,POS} \cdot d_{major} \tag{3}$$

with $K_{ffmd,POS}$ being conservatively set to 10 according to the current standards (RTCA, 2017b). However, this value is likely to change and be reduced, as we already discussed and suggested in previous work (Jochems et al., 2022). The parameter d_{major} describes the size of the semi-major axis of the error ellipse. The details for the calculation can be found in DO-253D and were also discussed by Jochems et al. (2022). The faulted protection level $HPL_{H1,j}$ is calculated as

$$HPL_{H1,j} = \left|B_{horz,j}\right| + K_{md,POS} \cdot d_{major,H1}. \tag{4}$$

The horizontal B-values ($B_{horz,j}$) are calculated based on the B-values transmitted in the GBAS message, $K_{md,POS}$ is again the missed detection multiplier set to 5.3 for the H1-case and $d_{major,H1}$ is again the semi major axis of the error ellipse, differing from the nominal d_{major} only by an inflated ground noise component accounting for the potentially faulted reference receiver. Finally, HEB is calculated as

$$HEB = \max\left\{\mathrm{HEB_j}\right\} \tag{5}$$

with

$$HEB_j = \left|s_{horizontal,j}\right| \cdot x_{air} \cdot P_j + K_{md,e,pos} \cdot d_{major} \tag{6}$$

and $s_{horizontal,j}$ being the horizontal s-values, x_{air} the distance between the GBAS reference point and the user, P_j the ephemeris decorrelation parameter transmitted in the GBAS message, the missed detection multiplier for the ephemeris bound $K_{md,e,pos}$ set to 4.1 and d_{major} again the semi major axis of the error ellipse. For all calculations of the error ellipses, the nominal and standardized σ_{air} describing the residual noise and multipath errors for 100 seconds smoothed pseudoranges were used.

Finally, the horizontal protection levels for SBAS and the GBAS positioning service are compared. The vertical protection level (VPL) performance is currently not shown because for the GBAS positioning service no VPLs are defined (as it was envisioned for large aircraft that would rely on barometric altimetry).

3. RESULTS

In this section, the results of the flight test and performance evaluations are shown. As described, the results were obtained by post processing flight test GNSS recordings and GBAS message recordings using the PEGASUS software tool. First, the standard smoothing time of 100 s was used, in a second run the smoothing time was set to 10 s in the advanced settings of PEGASUS.

3.1 GBAS DATA FLIGHT TRACK

The broadcast of the GBAS data was received with a software defined radio and then converted into the PEGASUS format for subsequent post processing. Figure 2 shows on the left side the broadcast pseudorange corrections (PRC) for the satellites in view. The corrections vary from about -33 m to just above +10 m. The very large corrections (in absolute terms) correspond to rising or setting satellites at low elevations. The jumps in the corrections occur at epochs when a satellite is added or removed from the set of corrections. The right part of Figure 2 shows the broadcast values for $\sigma_{\mathrm{pr,gnd}}$, i.e. the residual error estimates for the pseudorange corrections. For most of time, these vary between +0.26 m and +0.3 m, except for the low elevation satellites shortly after rising or just before setting.

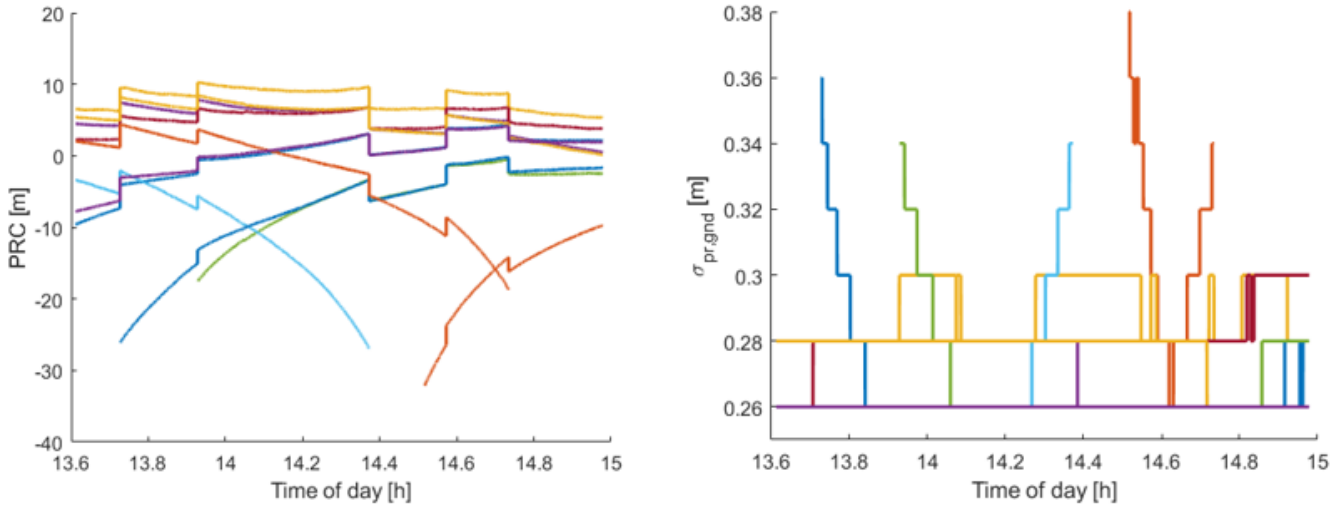

Figure 2 *Plot on the left: Pseudorange Corrections (PRCs); Plot on the right: Corresponding $\sigma_{pr,gnd}$ values, received from the GBAS ground station at Zurich Airport. Each color represents a satellite.*

Figure 3 *Rectangular flight tracks on the glider airfield in Winterthur. The green line shows the GBAS solution using a smoothing time constant of 10 s, the red line shows the SBAS solution.*

Figure 3 shows the ground track of the flight at the glider airfield in Winterthur. First the smaller rectangle was flown, subsequently the larger one. At each of the corners the UAV was kept stationary for 3 minutes before flying the next leg of the pattern. The green line shows the track of the GBAS solution, while the red line shows the track of the SBAS solution. The flight was conducted at a height of 15 m above ground.

3.2 NUMBER OF USED SATELLITES

The number of used satellites throughout the flight for different processing modes is shown in Figure 4. The left part of the plot until about 14.2 h shows data when the UAV was hovering stationary and was only climbing to the two different heights above ground for the multipath assessment (see next subsection). The right part corresponds to the scenario when the UAV was flown more dynamically in a rectangular pattern. Starting from the top in the image, the black dashed line shows the number of satellites that are visible at the time of the flight, using a 5 ° elevation mask and thus correspond to the theoretical maximum number of usable satellites. Note that GBAS and SBAS only provide corrections for GPS, thus the number of satellites shown here does not include visible satellites from other constellations. The green line shows the number of satellites used in the SBAS solution. In the first part of the flight, the SBAS solution uses either the number of satellites visible or one (for very short periods also two) satellite less than that.

In the right part of the plot where the flight was conducted in a more dynamic way, the number of used satellites drops to a minimum of just 6 out of 10 usable satellites at the end of the flight and results thus a larger difference between the used and the available satellites. The blue and the red curve show the number of satellites used for the GBAS solution using smoothing time constants of 100 s and 10 s, respectively. The most striking feature is the constant oscillating behavior of including and excluding one satellite from the solution. This behavior is not typical for GBAS. However, in the processing chain several monitors are active to detect and exclude any abnormal measurements. In our case, the most likely reason for this oscillation is an issue with the recording and decoding of the data leading to delayed messages that let the processing to exclude satellites. However, looking at the upper limit of the constantly changing data, the pattern in the left part of the plot is similar to that of SBAS for the 10 s smoothing time constant. For the 100 s smoothing time constant, the pattern is similar but with a significant time lag due to the smoothing filter convergence time. In the right part of the plot whit the more dynamic maneuvers, the 10 s smoothed GBAS solution and the SBAS solution again show a similar behavior with GBAS occasionally excluding one satellite more. However, the blue curve showing the results for the 100 s smoothed GBAS solution shows a significant drop to just 5 satellites (again as the upper limit without the frequent exclusions) and even just 4 satellites towards the very end. For this reason, the further evaluations regarding positioning performance in section 3.5 are based on the 10 s smoothed GBAS data.

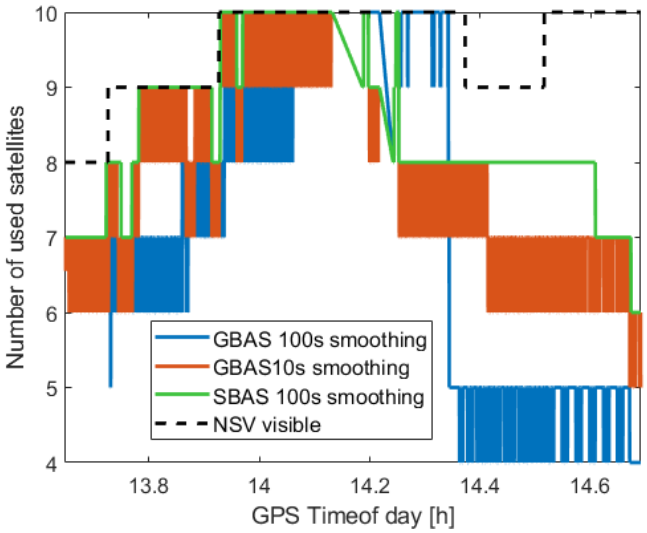

Figure 4 *Number of visible satellites (black dashed line) and number of used satellites for SBAS (green), GBAS with 100 s smoothing (blue) and 10 s smoothing (red).*

3.3 MULTIPATH PERFORMANCE AS A FUNCTION OF FLIGHT ALTITUDE

To analyze the differences in multipath in relation to the height of the drone above ground, the standard deviation of the multipath was calculated. This was done per satellite and was then visualized as a function of the average elevation during the few minutes where data was collected. The left plot in Figure 5 shows the standard deviations of every satellite for smoothing time constants of 10 seconds (triangles) and 100 seconds (points) for every average elevation angle of each satellite while hovering at an altitude of 2 m above ground. The standardized airborne multipath model (black crosses and line) is shown for comparison. The same data is shown for the flight period at 5 m above ground in the right plot of Figure 5.

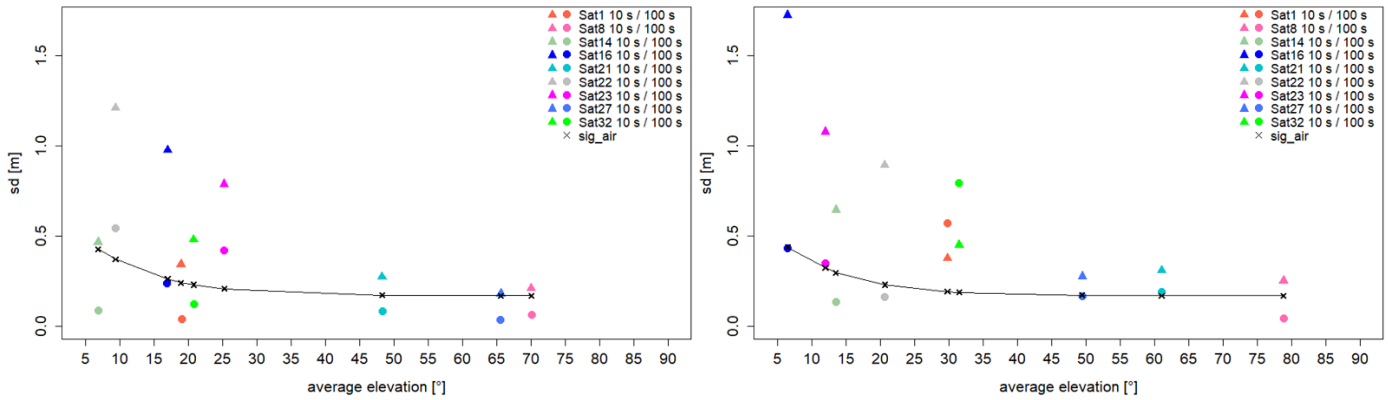

Figure 5 *Multipath performance as a function of average elevation at a flight altitude of 2 m (left plot) / 5 m (right plot) above ground after 10 s (triangles) and 100 s (points) smoothing. Black crosses represent the computed σ_{air}, the colors correspond to the individual satellites as indicated in the legend.*

In the case of hovering at 2 m above ground (plot on the left side), it is clearly visible that the standard deviation after 10 seconds of pseudorange smoothing is always significantly higher than that after 100 seconds of smoothing. Also, a decreasing trend of the standard deviations with increasing average elevation angles is visible, especially in case of 10 s smoothing. The 100 s smoothed multipath estimates are mostly very well in line with the standardized airborne multipath models, while the data using only 10 s of smoothing significantly exceeds the curve. For an altitude of 5 m above ground (plot on the right), the generally higher values after 10 seconds of smoothing (with the exception of PRN 1 and PRN 32) as well as the decreasing trend of the standard deviations with increasing satellite elevation are visible again. In comparison to the multipath performance at 2 m above ground, the standard deviation of the satellite at just over 5 ° elevation (PRN 16) after 10 seconds of smoothing (triangle in dark blue) is significantly higher. Most other satellites show a more modest increase but indicate an increasing trend compared to the data from just 2 m above ground.

3.4 HORIZONTAL PROTECTION LEVEL PERFORMANCE (GBAS / SBAS)

In order to evaluate the potential benefit of applying GBAS corrections during a drone flight, $HPL_{GBAS,pos}$ was compared against the SBAS horizontal protection level (HPL_{SBAS}). The two graphs below in Figure 6 illustrate this comparison. On the left side of the figure, $HPL_{GBASpos}$ and HPL_{SBAS} are shown over the duration of the flight test. $HPL_{GBASpos}$ is illustrated with black points, HPL_{SBAS} with red points. As before, the first part until about 14.2 h shows data when the UAV was hovering stationary, afterwards the UAV was flown in a more dynamic way. During the gap in the middle the UAV was moved and repositioned, therefore no GBAS/SBAS position solutions were calculated. It is clearly visible that the GBAS HPL is generally significantly lower than the SBAS HPL. Only towards the end there are several instances where $HPL_{GBAS,pos}$ becomes larger than HPL_{SBAS}. Moreover, the protection levels are larger in the second part of the flight test (right side of the left plot) than during the stationary hovering of the UAV. This is especially visible in case of the SBAS protection level and corresponds well to the lower number of usable satellites shown in the previous section.

The times at which the significant and frequent jumps in the $HPL_{GBAS,pos}$ occur coincide with the times at which the number of used satellites changes. This can be seen by comparing the left plot in Figure 6 with the graph shown in Figure 4. One example for this is at around 13.9 h, where the GBAS and SBAS HPL drop down from around 3.7 to 3.0 m ($HPL_{GBASpos}$) and around 9 to 7.8 m (HPL_{SBAS}). At this time, the number of used satellites increases from 8 to 9 satellites. Again, the frequent loss and recovery of individual satellites is likely caused by the GBAS message decoding and is not a GBAS-specific behavior.
The right side of Figure 6 shows a histogram of the GBAS and SBAS protection levels. The GBAS protection level is represented by the blue bars, the green bars show the SBAS horizontal protection level. The vertical lines in dark blue and dark green visualize the median of the $HPL_{GBASpos}$ and the HPL_{SBAS}, respectively. The former lies at 3.9 m, the latter at 9.8 m. Again, it is clearly recognizable that most of the time the GBAS horizontal protection levels are substantially smaller than the SBAS protection levels.

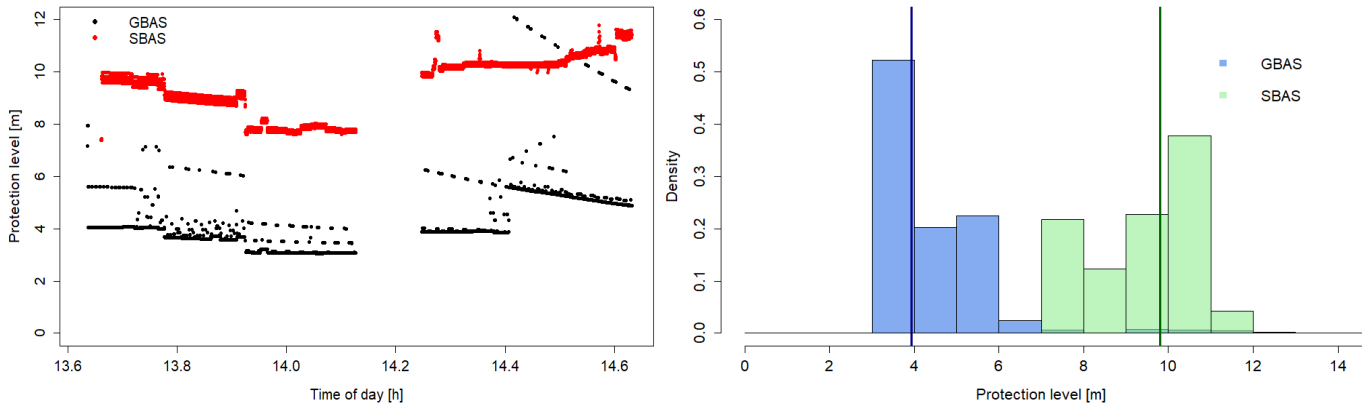

Figure 6 *Plot on the left: GBAS and SBAS horizontal protection level in meters over the course of the flight test. The black points show the GBAS HPL, the red points represent the SBAS HPL; Plot on the right: Histogram of GBAS and SBAS horizontal protection level in meters. GBAS HPL is represented by the blue bars, SBAS HPL by the green bars. The vertical lines in dark blue and dark green show the median of the GBAS HPL and SBAS HPL, respectively.*

3.5 COMPARISON TO REFERENCE TRAJECTORY

In the previous sections, the multipath as well as the protection level performance were evaluated. Finally, the accuracy of the GBAS and SBAS augmented solutions is assessed by comparing it to a post-processed differential carrier phase reference trajectory. All results in this section are based on a smoothing time of 10 s for the GBAS corrected flight path.

Figure 7 shows the position error for the dynamic flight part in meters in East, North and vertical direction over the course of the flight test. The red, blue and green points illustrate the error component in East, North and vertical direction, respectively. The size of the error varies between -3 and +5 meters. While the errors in North and vertical direction scatter strongly, the East error varies mostly between approximately 0 and +1 m. This can be confirmed by looking at the histogram shown in Figure 8, which also shows the data of the dynamic flight. Most of the errors in easterly direction lie within -0.5 and +1.5 meters with only a few outliers up to +3.8 meters. The majority of the errors in North direction range from -2.0 to +2.5 meters, exceptionally reaching values of up to +3.4 meters. The errors in vertical direction have the largest range – from -3 to +4.5 meters. However, most of the values lie between -1 and +4 meters.

TABLE 1

Mean and Standard Deviation of the error components in East, North and vertical direction during the dynamic flight testing

	East	North	Vertical
Mean [m]	+0.57	-0.12	+1.37
Standard deviation [m]	+0.49	+0.90	+1.32

Table 1 shows the mean and standard deviation of the error components in East, North and vertical direction during the dynamic flight testing. The values validate the previous statements: the error in East direction has the smallest standard deviation, which therefore confirms the lowest spread. The mean of the error component in North direction lies with -0.12 m very close to 0, however the standard deviation of +0.90 m indicates larger scattering of the values. The error in vertical direction has the largest mean and standard deviation out of the three error components.

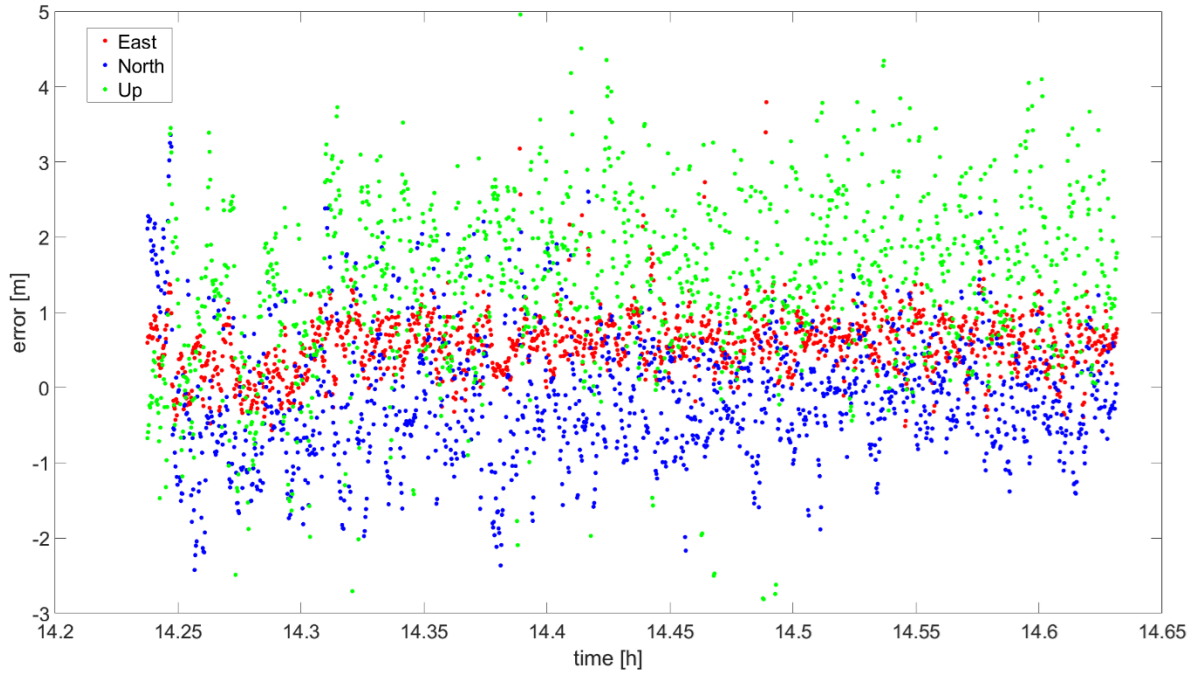

Figure 7 *Calculated position in ENU-coordinates. The local origin is the reference trajectory. The y-axis shows the error in meters, the x-axis depicts the time of day in hours. Red, blue and green points represent the error component in East, North and vertical direction, respectively.*

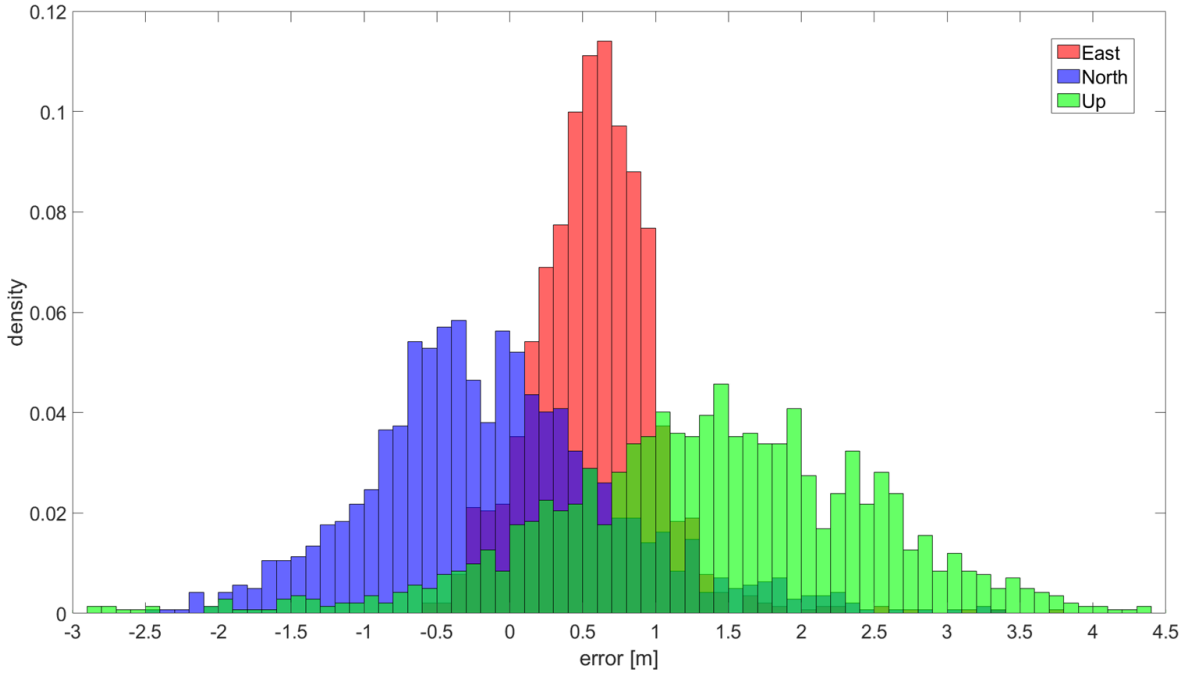

Figure 8 *Histogram of the position errors in East, North and vertical direction. The x-axis shows the position error in meters, on the y-axis the density is depicted. Red, blue and green bars represent the error component in East, North and vertical direction, respectively.*

Figure 9 depicts the horizontal error over the time of the flight (dynamic part). The x-axis shows the time of the day in hours, the y-axis shows the horizontal error in meters. The error ranges from +0.06 m to +3.8 m.

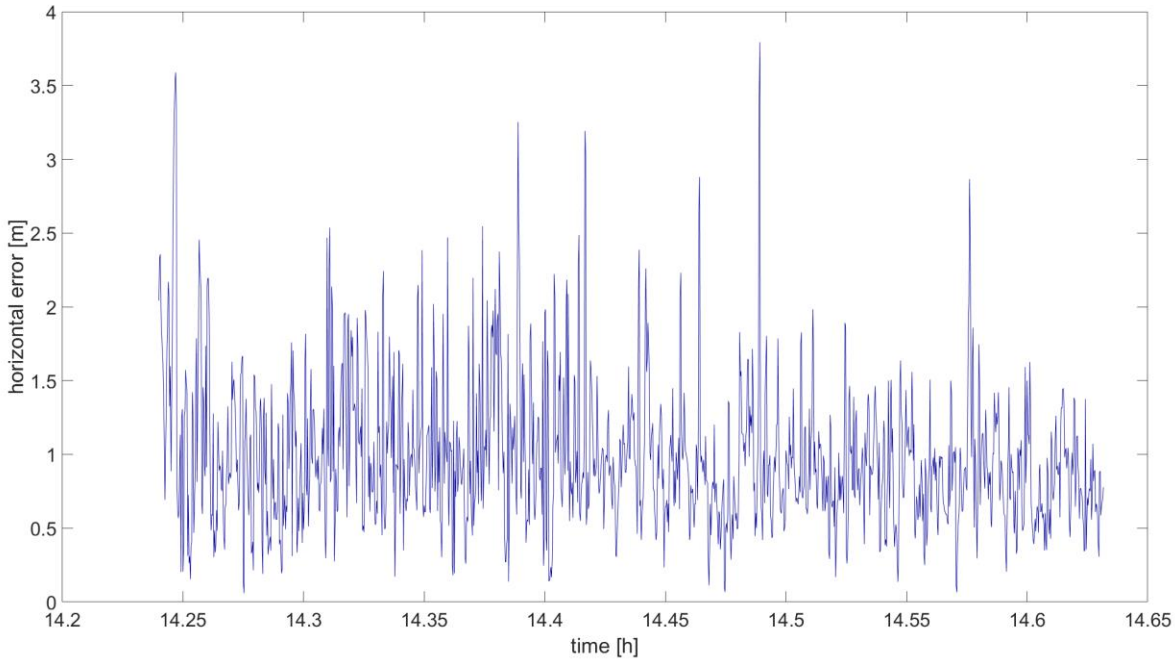

Figure 9 *Horizontal error in meters over the course of the dynamic flight part.*

The values of the horizontal error are mostly between 0 and +2.5 m with a only a few outliers lying above that. This can be seen in the histogram shown in Figure 10.

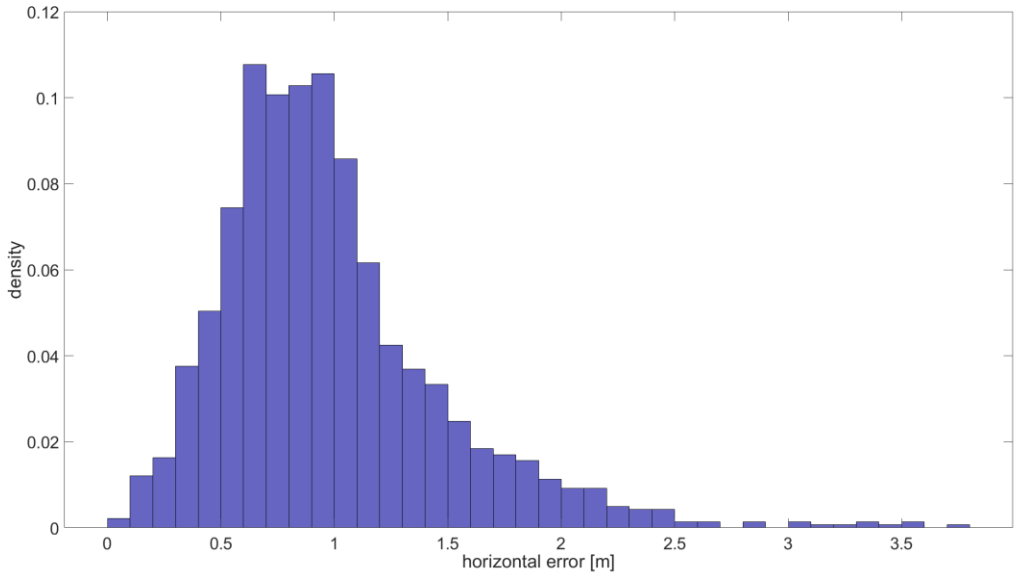

Figure 10 *Histogram of the horizontal error. The x-axis depicts the horizontal error in meters, the y-axis shows the density.*

4. DISCUSSION

This section discusses the obtained results and puts the various influences such as number of used satellites, smoothing time and attitude of the drone into context.

4.1 FLIGHT PROFILE, MANEUVERING AND EQUIPMENT

The flight was conducted at a height of 15 m above ground, which is a rather low altitude. Higher altitudes may experience less impact from multipath and would be preferrable from that perspective. In general, the dynamics and attitude changes of UAVs are much more significant than those of large transport aircraft. Furthermore, the antenna and receivers used on UAVs tend to be smaller and often show performance worse than that of operational and certified avionics on board of large aircraft. This may lead to larger errors stemming from increased noise and potentially larger errors induced by antenna group delay as discussed e.g. by Caizzone et al. (2019).

4.2 NUMBER OF USED SATELLITES AND SMOOTHING TIME

Figure 4 in section 3.2 shows that there is a significant difference between the 10 s ($GBAS_{10s}$) and 100 s smoothed GBAS data ($GBAS_{100s}$) as $GBAS_{100s}$ uses 1 to 2 satellites (in a static scenario) and up to 3 satellites (dynamic flight) less than $GBAS_{10s}$ at the same time. Dynamic maneuvers cause large and sudden changes in the attitude of the UAV and thus lead to frequent loss of tracking of individual satellites. This leads to the position solution being calculated based on very few satellites and to increased errors and larger protection levels due to the weaker satellite geometries. As mentioned in the beginning, in this case the smoothing filter needs to be re-initialized. After (re-)initialization of the smoothing filer it takes 3.6 times the smoothing time constant until the filter has converged. Currently, avionics manufacturers (re-)include satellites much quicker but inflate the corresponding σ_{air} for that satellite. PEGASUS does not do this but waits for filter convergence before (re-)inclusion of the satellite into the position solution. In the case of 100 s of smoothing, this corresponds to a time of 6 minutes a satellite has to be tracked continuously before it is used. As we were only hovering for about 3 minutes at the corners of the rectangle, the processing did not have enough time to re-incorporate all lost satellites into the position solution. When setting the smoothing time filter constant to 10 s, PEGASUS re-incorporates the lost satellites after just 36 seconds leading to more available satellites for navigation purposes. For operational purposes, however, this is not a feasible solution since the mismatch in smoothing time constant between the airborne measurements and the PRCs generated on the ground can lead to the build-up of differential errors that are of course to be avoided. Two practicable solutions for this issue may be a faster (re-)inclusion of satellites with an inflation of the corresponding σ_{air}, and/or placing the GNSS antenna on a gimbal to avoid loss of tracking in the first place.

4.3 MULTIPATH PERFORMANCE

The amount of residual multipath in the position solution depends to a large degree on the amount of multipath affecting the measurements in the first place and subsequently on the smoothing filter used to reduce the impact. While residual errors on pseudoranges after 100 s of smoothing are well in line with the standardized airborne multipath models, the data using only 10 s of smoothing considerably exceeds the models and a significant amount of residual noise and multipath persists in the position solution. These findings are consistent with the airborne multipath assessments for UAVs done by Kim et al. (2015) and the discussion about smoothing filter convergence by Circiu et al. (2015). The airframe itself does likely not cause reflections more severe than that of a large transport aircraft, however UAVs come in a great variety of different shapes and sizes so such a claim should be investigated for each type of aerial vehicle.

Typical altitudes at which UAVs operate tend to be high enough to not be influenced by ground reflections anymore. However, when operating close to the ground, especially during take-off and landing, this might not be true anymore and more multipath can affect the airborne receiver. In general, it seems to be reasonable and confirmed by the indicative results in this work to assume that the σ_{air} values derived for large transport aircraft can also bound multipath errors in UAV operations. However, the variety of UAVs, GNSS antenna and receiver installation and performance can differ significantly, and the potential area of operations are wide. Thus, it is challenging to generate and use a one-size-fits-all model for the airborne multipath that holds in all scenarios.

4.4 GBAS AND SBAS PROTECTION LEVEL PERFORMANCE

Safely bounding residual errors is a critical step when using GNSS for safety-critical applications. This is achieved by the calculation of protection levels. GBAS provides locally generated corrections and integrity parameters, while SBAS provides correction and integrity parameters on a continental scale. Close to the GBAS, it was confirmed in this study that the protection levels for GBAS are significantly smaller than those bounding the residual SBAS errors (for our trial the HPLs for GBAS were roughly on the order of 5 m while for SBAS these values were on the order of roughly 10 m). The distance between our UAV flight test and the

GBAS at Zurich airport was approximately 15 km and thus rather close to airport and within the specified GBAS service area where good performance could be expected.

In general, the proposed approach to receive and decode GBAS messages somewhere at the airport and apply them to users that cannot directly receive the VDB data broadcast of the ground station worked well. However, GBAS by design uses a number of different monitors and integrity checks to ensure correct reception of the messages and validity of the data contained. In our setup, the message decoding was likely not always timely and valid causing frequent exclusions and re-inclusions of satellites into the position solution that is not desirable from an operational perspective.

Finally, the protection levels significantly depend on the geometry of the satellites available for calculating a position solution. The large attitude angles and frequent attitude changes of a drone in flight together with the necessary smoothing and the time for the smoothing filter to converge reduce the number of available satellites significantly and thus impacts the protection level performance. The situation may further worsen for scenarios where a drone is landing, and part of the sky may be blocked by obstacles in the vicinity of the landing site.

4.5 POSITIONING ACCURACY

Another very important performance parameter is, of course, the accuracy of the position solution. For determining the GBAS positioning errors we calculated a reference trajectory and compared the results against it. The horizontal errors mainly stayed within the range of 0 to +2.5 m with a standard deviation of 0.62 m. It should be noted and emphasized here again, that we chose to present the results regarding accuracy based on the 10 s smoothed pseudoranges as the number of available satellites using 100 s smoothing would be so small that no really meaningful performance assessments could be made due to poor geometry for most of the dynamic part of the flight with 5 or 4 satellites or even less so that no position solution could be calculated at all. Hence, the residual noise and multipath in the results is significantly larger (see performance comparison in section 3.3) than it would be using the 100 s smoothing that is standard for GBAS and SBAS. It should further be noted here that no meaningful comparison between the accuracy (based on 10 s smoothing) and the protection level error bounds (based on multipath models bounding residual errors after 100 s smoothing) can be made in this case.

5. CONCLUSIONS

In this study we showed a proof of concept for using GBAS corrections from an operational ground station for different applications than guiding large aircraft on the final approach, in our case navigating a UAV. One main challenge for such new applications is the possibility to receive the broadcast corrections as for VHF communications near line-of-sight must be given to ensure reception. This is typically not the case for UAV operations, so the concept explored is to receive, decode and forward the GBAS messages by other means than the VDB broadcast, such as via the cellphone network. Receiving, timely decoding and forwarding of the messages is possible in principle, however we experienced some challenges regarding that task resulting in frequent undesirable satellite exclusions. A more significant problem were the frequent and significant changes of attitude angle of the airborne UAV. This led to loss of tracking of many satellites and required a re-initialization of the smoothing filter. Waiting for filter convergence takes a long time, especially when using a 100 s smoothing filter as required when using GBAS corrections. Therefore, for such kinds of operations it is necessary to re-include satellites much faster back into the position solution so that satisfactory performance can be achieved. For this issue, using multiple constellations and therefore having significantly more satellites available would greatly improve the performance and reduce the impact of losing satellites. Another way to avoid loss of tracking in the first place would be to mount the antenna on a gimbal on top of the UAV so that the antenna is not tilted with the aircraft when maneuvering.

ACKNOWLEDGMENTS

The results presented in this paper were developed within a project funded by Swiss FOCA under grant number SFLV2019-038. The authors would like to thank the FOCA for their funding and support for the topic.

REFERENCES

Caizzone, S., Circiu, M. S., Elmarissi, W., Enneking, C., Felux, M., & Yinusa, K. (2019). Antenna influence on GNSS pseudorange performance for future aeronautics multifrequency standardization. *NAVIGATION*, 66(1), 99-116. https://doi.org/10.1002/navi.281

Circiu, M. S., Caizzone, S., Felux, M., Enneking, C., Rippl, M., & Meurer, M. (2020). Development of the dual-frequency dual-constellation airborne multipath models. *NAVIGATION*, 67(1), 61-81. https://doi.org/10.1002/navi.344

Circiu, M. S., Felux, M., Belabbas, B., Meurer, M., Lee, J., Kim, M., & Pullen, S. (2015, September). Evaluation of GPS L5, Galileo E1 and Galileo E5a performance in flight trials for multi frequency multi constellation GBAS. In Proceedings of the 28th International Technical Meeting of The Satellite Division of the Institute of Navigation (ION GNSS+ 2015) (pp. 897-906).

Hatch, R. (1983). The synergism of GPS code and carrier measurements. *International geodetic symposium on satellite doppler positioning* (Vol. 2, pp. 1213-1231).

Jochems, S., Felux, M., Schnüriger, P., Jäger, M., & Sarperi, L. (2022, January). GBAS use cases beyond what was envisioned–drone navigation. *Proc. of the 2022 International Technical Meeting of The Institute of Navigation* (pp. 310-320), https://doi.org/10.33012/2022.18213

Kim, M., Kim, K., Lee, D. K., & Lee, J. (2015). GNSS Airborne Multipath Error Modeling Under UAV Platform and Operating Environment. *Journal of Positioning, Navigation, and Timing*, 4(1), 1-7. https://doi.org/10.11003/JPNT.2015.4.1.001

Murphy, T., Harris, M., Geren, P., Pankaskie, T., Clark, B., & Burns, J. (2005, September). More results from the investigation of airborne multipath errors. *Proc. of the 18th International Technical Meeting of the Satellite Division of The Institute of Navigation (ION GNSS 2005)* (pp. 2670-2687).

Pullen, S., Enge, P., & Lee, J. (2013a). High-integrity local-area differential GNSS architectures optimized to support UAVs (Unmanned Aerial Vehicles). *Proc. of the 2013 International Technical Meeting of The Institute of Navigation*

Pullen, S. (2013b). Managing separation of unmanned aerial vehicles using high-integrity GNSS navigation. *Proc. EIWAC 2013*, 19-21.

RTCA (2017a), *GNSS-Based Precision Approach Local Area Augmentation System (LAAS) Signal-in-Space Interface Control Document (ICD)* (DO-246E). https://www.rtca.org/

RTCA (2017b), *Minimum Operational Performance Standards for GPS Local Area Augmentation System Airborne Equipment* (DO-253D). https://www.rtca.org/

RTCA (2020), *MOPS for Global Positioning System/Satellite-Based Augmentation System Airborne Equipment* (DO-229F). https://www.rtca.org/